Carbohydrate Polymers 295 (2022) 119885

Contents lists available at ScienceDirect

Carbohydrate Polymers

journal homepage: www.elsevier.com/locate/carbpol

Morphological and rheological properties of cellulose nanofibrils prepared by post-fibrillation endoglucanase treatment

Xiaojun Wang [a,b], Jinsong Zeng [b,c,*], J.Y. Zhu [d,**]

[a] State Key Laboratory of Bio-Fibers and Eco-Textiles, Qingdao University, No. 308 Ningxia Road, Qingdao 266071, PR China
[b] State Key Laboratory of Pulp and Paper Engineering, Plant fiber Research Center, School of Light Industry and Engineering, South China University of Technology, Guangzhou 510640, China
[c] Guangdong Plant Fiber High-Valued Cleaning Utilization Engineering Technology Research Center, South China University of Technology, Guangzhou 510640, China
[d] Forest Products Laboratory, U.S. Department of Agriculture, Madison 53726, USA

ARTICLE INFO

Keywords:
Post-fibrillation enzymatic treatment
Cellulose nanofibrils
Morphology
Suspension rheology
Endoglucanase

ABSTRACT

Post-fibrillation endoglucanase treatment was employed to reduce the entanglement of cellulose nanofibrils (CNFs) produced with low extent of mechanical milling. The results showed that post-fibrillation endoglucanase treatment can effectively reduce the fibril degree of polymerization (DP) values and therefore entanglement. Cellulose DP was reduced from 520 for CNFs prepared by milling using a SuperMassColloider with 1 pass to 225 after endoglucanase treatment at a low dosage of 1 mg protein/g fibril for 24 h. Endoglucanase treatment can also effectively reduce the fibril mean diameter from 66 nm to 25 nm. Applying post-fibrillation endoglucanase treatment produced more uniform CNFs than the feed CNFs from pure mechanical treatment. All CNFs suspensions prepared by post-fibrillation endoglucanase treatment were non-Newtonian (except at very low concentrations below 0.5 wt%) with shear thinning behavior. Post-fibrillation endoglucanase treatment reduced the viscosity of CNF suspensions due to decreasing fibril DP values and the extent of entanglement.

1. Introduction

Lignocellulose is the most abundant, renewable, and low-cost natural resource (Li, Chen, et al., 2021). However, only a fraction of this resource is valorized, such as for papermaking. Cellulose as the main component of lignocellulose is biodegradable (Mandal & Chakrabarty, 2011; Questell-Santiago, Zambrano-Varela, Amiri, & Luterbacher, 2018). Cellulose nanomaterials (CNMs), which include microfibrillated cellulose (MFC), cellulose nanofibrils (CNFs), and cellulose nanocrystals (CNCs), derived from cellulosic materials have excellent properties, such as low density, low thermal expansion, great specific surface area, biocompatibility, and high mechanical strength (Sacui et al., 2014; Wan, Lian, Wang, & Ma, 2015). Therefore, CNMs have potential for a variety of applications (Li, Chen, et al., 2021), such as in papers (Yousefi, Azad, Mashkour, & Khazaeian, 2018) and composites (Aarstad et al., 2017), medicine formulation (Khan, Wang, & Ni, 2020), electronics (Williams, Bullard, Brooke, Therien, & Franklin, 2021), etc. However, sustainable production of CNMs from raw lignocellulose or commercial pulp fiber remains a challenge despite wide applications having been reported. Chemical pretreatments using existing technologies to reduce fibrillation energy may raise environmental concerns (Zhu et al., 2021). Usage of large amounts of water due to processing at low solids loadings is another concern. Although lignocellulosic biomass can be sustainably produced in large quantities, CNMs can be considered sustainable only when the production process can achieve economic and environmental sustainability.

Mechanical fibrillation is the most common method for producing CNFs. Disk milling, such as using a SuperMassColloider (SMC), has been widely used for its commercial scalability (Hu, Zhao, Li, Zhu, & Gleisner, 2015; Iwamoto, Nakagaito, & Yano, 2007; Wang et al., 2012). However, the main disadvantage of pure mechanical fibrillation is high energy consumption due to the strong recalcitrance of cell walls to deconstruction into nanofibrils (Hoeger et al., 2013; Spence, Venditti, Rojas, Habibi, & Pawlak, 2011; Wang et al., 2012). Pretreatment of fibers using chemicals (Bian, Chen, Gleisner, Dai, & Zhu, 2017; Cai et al., 2020; Qin, Qiu, & Zhu, 2016; Saito et al., 2009; Wang, Chen, Zhu, & Yang, 2017) or

* Correspondence to: J. Zeng, Guangdong Plant Fiber High-Valued Cleaning Utilization Engineering Technology Research Center, South China University of Technology, Guangzhou 510640, China.
** Corresponding author.
E-mail addresses: fezengjs@scut.edu.cn (J. Zeng), junyong.zhu@usda.gov (J.Y. Zhu).

https://doi.org/10.1016/j.carbpol.2022.119885
Received 8 April 2022; Received in revised form 12 July 2022; Accepted 15 July 2022
Available online 20 July 2022

enzymes (Anderson et al., 2014; Arantes et al., 2020; Filson, Dawson-Andoh, & Schwegler-Berry, 2009; Henriksson, Henriksson, Berglund, & Lindstrom, 2007; Hu, Tian, Renneckar, & Saddler, 2018; Koskela et al., 2019; Paakko et al., 2007; Tenhunen et al., 2014; Wang et al., 2016; Zhou, St John, & Zhu, 2019) can substantially reduce energy input. Comparing with chemical treatment, enzymatic treatment has advantages of eliminating chemical recovery with minimal environmental impact. It has been reported that enzymatic pretreatment primarily depolymerizes cellulose to decrease cellulosic fiber length to facilitate subsequent fibrillation for producing thin diameter fibrils (Henriksson et al., 2007; Paakko et al., 2007; Zhu, Sabo, & Luo, 2011). Recently, post-fibrillation enzymatic treatment received interest for its ability to tune the morphology of the resultant fibrils (Gourlay, Van Der Zwan, Shourav, & Saddler, 2018; Wang et al., 2016; Wang et al., 2020; Xu et al., 2021). Post-fibrillation endoglucanase treatment depolymerizes cellulose through cleaving the β-1-4 glycosidic bond to result in decreasing fibril network entanglement and aggregations (Bian et al., 2019; Gourlay et al., 2018; Wang et al., 2016). Limited data showed that post-fibrillation endoglucanase treatment with (by its definition) no subsequent mechanical fibrillation also resulted in thinner diameters (Wang et al., 2016). Limited data showed that the morphological change by post-fibrillation endoglucanase treatment also decreased fibril suspension viscosity as demonstrated in a narrow shear rate range (Gourlay et al., 2018). However, earlier studies did not provide understanding of how mere cellulose depolymerization (fibril longitudal direction) by post-fibrillation endoglucanase treatment can decrease fibril diameters. Furthermore, it is unclear how the fibril interactions through entanglement or forming fibril network under various fibril concentrations affect the suspension rheological properties. Moreover, no comparative studies on energy consumptions between enzymatic pretreatment and post-fibrillation enzymatic treatment were reported for producing fibrils with equivalent morphologies.

CNF suspensions have been identified as an effective rheological modifier for a variety of applications such as food and cosmetics (Heggset et al., 2020), oil drilling fluids (Li, Wu, Moon, Hubbe, & Bortner, 2021; Villada et al., 2021), coating and painting (Liu et al., 2017), etc. Many studies have been conducted on rheological properties of CNF suspensions (Li et al., 2015; Liao, Pham, & Breedveld, 2021; Nechyporchuk, Belgacem, & Pignon, 2016). Although, one can always change the suspension consistency or CNF loading in rheology modification using CNFs, it is desirable to be able to modify rheology at a constant CNF loading. This requires tuning the rheological properties of CNF suspensions in a range of CNF concentrations and shear conditions. Developing a complete understanding of post-fibrillation enzymatic treatment on modifying the rheological properties of CNF suspensions can fill this gap. The objective of this study is to conduct a detailed exploration of the effects of post-fibrillation endoglucanase treatment on the rheological properties of the resultant CNF suspensions under a broad range of operating conditions that were not reported in literature. The effect of post-fibrillation endoglucanase treatment on CNF morphology was examined, along with the characterizations of the resultant CNF cellulose degree of polymerization (DP), crystallinity (CrI), and CNF water retention value (WRV), a measure of CNF degree of fibrillation (Gu et al., 2018). By examining the rheological properties of CNF suspensions in both steady and dynamic conditions, the enzymatic modification of fibril morphology on fibril interactions and therefore suspension flow structure and rheology behavior were revealed. With the advances in enzymology, especially those on tailoring enzymes for producing cellulose nanomaterials (Anderson et al., 2014; Arantes et al., 2020; Hu et al., 2018; Koskela et al., 2019; Squinca, Bilatto, Badino, & Farinas, 2020; Yarbrough et al., 2017), post-fibrillation enzymatic treatment can be an effective and sustainable processing technology for producing next-generation cellulose nanomaterials (Arantes et al., 2020).

2. Materials and methods

2.1. Materials

Bleached hardwood kraft pulp (BHKP) with DP of 650 was supplied by a mill in Shandong province, China. Endoglucanase Banzyme 2900 was purchased from UPM-Kymmene Co., Ltd. (Jiangsu, China). Enzyme activity of Banzyme 2900 was 7.3 IU/mL and its protein content was 162.0 mg/g. Cupriethylenediamine hydroxide solution was purchased from Aladdin Co., Ltd. (Shanghai, China). Bovine serum protein and other chemicals were supplied by Macklin Biochemical Co., Ltd. (Shanghai, China).

2.2. Post-fibrillation endoglucanase treatment of CNFs

As shown in Fig. 1, BHKP was first milled by a SMC (MKZCA 6-2 J, Masuko Sangyo Co., Ltd., Japan), followed by endoglucanase treatment. To prevent blockage in milling, BHKP suspension at solid loading of 1 wt % was first milled using a set of coarse disks (E6-46DD) for one pass sequentially at each disk plate gap of +20, 0, −20 and − 100 μm. The resultant sample was labelled as CsP1. Then, CsP1 was subjected to fine milling using a set of fine disks with plate pattern GC6-80SD for one pass sequentially at each of the three disk-plate gap of +20, 0, −20 μm, followed by milling for varied passes of *n* at disk-plate gap of −100 μm. The acquired samples were labelled as FiP*n*.

Post-fibrillation endoglucanase treatment of SMC fine-milled fibrils FiP*n* was carried out at 50 °C and 200 rpm for 3–72 h at 5 wt% solids loading. Endoglucanase dosage was in the range of 0.1–9 mg protein/g fibrils (abbreviated as mg/g). Endoglucanase treatment was performed in 50 mM citric acid/sodium citrate buffer at pH 5.5. At the end of endoglucanase treatment, the samples were heated at 90 °C for 15 min to deactivate endoglucanase. Then, the obtained CNFs, labelled as Po-P*n*E*x*t*yy* with Po-P*n* representing post-fibrillation endoglucanase treatment of fibrils from *n* passes of fine milling, E*x* and t*yy* being endoglucanase dosage in *x* mg/g and treatment durations in *yy* h, respectively, were separated from the supernatant by centrifugation and then stored in refrigerator at 4 °C for further analysis.

2.3. Endoglucanase pretreatment

For comparison, BHKP was also enzymatically pretreated by endoglucanase at 1 mg/g for 6, 12 and 24 h and then mechanically fibrillated by SMC. The conditions for endoglucanase treatment were the same as those described above for post-fibrillation endoglucanase treatment. The pretreated fiber samples, labelled as Pre-E1t*yy* with Pre representing pretreatment, E1 being endoglucanase dosage at 1 mg/g fibrils, and t*yy* standing for enzymatic pretreatment duration in *yy* h, were milled in the same SMC under the same conditions as those described earlier, i.e., coarse milling at each disk-plate gap of +20, 0, −20 and − 100 μm for one pass followed by fine milling at each disk-plate gap of +20, 0, −20 μm for one pass and varied passes at disk-plate gap of −100 μm using the fine disk plates. SMC fibrillated samples were labelled as Pre-E1t*yy*P*n* with *n* as the number of passes in fine grinding at the same disk plate gap of −100 μm.

2.4. Extent of cellulose hydrolysis by endoglucanase

CNF yield (Y) after endoglucanase treatment was determined according to Eq. (1),

$$Y = M_1/M_0 \times 100\% \quad (1)$$

where, M_0 and M_1 are oven dry mass of cellulose fibers before and after endoglucanase treatment.

Concentrations of monosaccharides and oligosaccharides from endoglucanase treatment were analyzed by ion chromatography (ICS-

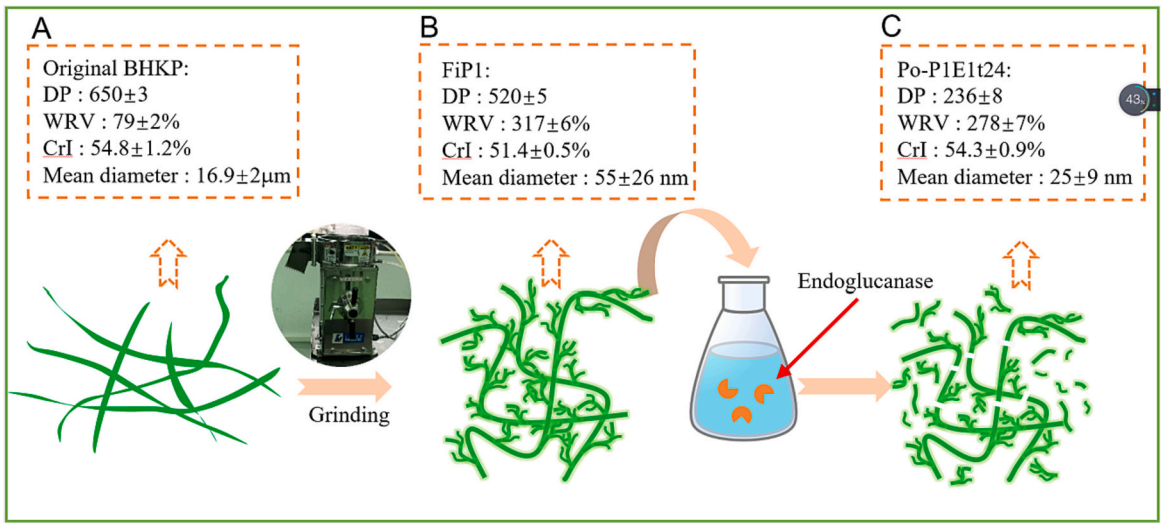

Fig. 1. A schematic flow diagram showing post-fibrillation endoglucanase treatment. (A) Original BHKP, (B) FiP1 obtained by SMC milling without enzymatic treatment (C) Po-P1E1t24 obtained by post-fibrillation endoglucanase treatment at dosage of 1 mg protein/g fibril for 24 h.

5000, Thermo Fisher scientific, USA). The hydrolysate was first centrifuged. Oligosaccharides in the supernatant were further hydrolyzed into monosaccharides based on quantitative acid hydrolysis using 4 % *w*/w of H_2SO_4 at 121 °C for 60 min (Sluiter et al., 2006). A 0.2 μm nylon syringe filter was employed to filter the supernatant prior to acid hydrolysis. The concentration of the oligosaccharides was determined from the difference between the monosaccharide concentrations before and after acid hydrolysis.

2.5. Characterization the extent of fibrillation, CNF morphology, size, and surface area

The extent of cellulose fiber fibrillation is characterized by the water retention value (WRV). Fiber or fibril samples were first soaked in water overnight. Then the soaked samples were wrapped in a 400 mesh filtration membrane and put into a centrifuge tube and centrifuged at 3000 *g* for 15 min (Gu et al., 2018). WRV was obtained according to Eq. (2),

$$\mathrm{WRV} = \frac{W_{wet} - W_{od}}{W_{od}} \times 100\% \quad (2)$$

where, W_{wet} was the wet weight of the sample after centrifugation and W_{od} was oven dry weight of the sample.

CNF morphologies were analyzed using scanning electron microscopic (SEM) imaging. An electron scanning microscope (Merlin, Germany) was operated at 0.05–30 kV. An aliquot of the diluted and well dispersed fibril suspension was dropped onto the newly split mica sheet and dried in air. The dried samples were coated with gold prior to imaging. Diameter measurements were carried out manually by randomly picking diameters from the obtained SEM images using software Nanomeasurer (Shanghai, China). The number of SEM images taken, used for diameter measurements, and number of diameters measured, is listed in Table S1. 69 to over 400 diameters were measured from the different milled fibrils to obtain statistical significance.

Transmittance of 0.1 wt% CNF suspensions was measured by a UV–vis spectrophotometer (UV-2600, Japan) in the wavelength range of 400–800 nm according to the reference with modifications (Sehaqui, Kulasinski, Pfenninger, Zimmermann, & Tingaut, 2017).

CNF surface area can be qualitatively characterized using enzyme adsorption (EA). Endoglucanase was added to 50 mL of CNF suspension at 1 wt% solids loading in a citric acid/sodium citrate buffer of pH 5.5. Endoglucanase dosage was 100 mg protein/g CNFs. Enzymatic adsorption was conducted in an air shaker (ZWYR-200D, China) at 20 °C and 200 rpm for 15 min. At the end of incubation, the CNF suspension was centrifuged at 5000 rpm for 10 min and the supernatant was collected. Protein content in the supernatant was measured by Bio-Rad method (Bradford, 1976). The amount of enzyme adsorption was determined from the difference in the protein content in the supernatant before and after adsorption.

2.6. Cellulose degree of polymerization (DP) and crystallinity

Cellulose DP was determined based on intrinsic viscosity measurements according to TAPPI T 230 OS-76 and SCAN–C 15:62 standards (Henrique et al., 2015). Accurately weighed cellulose sample was added into a brown glass bottle along with glass beads and a few copper sheets. 15 mL of distilled water was added and followed by shake violently to disperse the sample evenly. Then 15 mL of Cupriethylenediamine hydroxide solution was supplemented. The brown glass bottle was shaken energetically to completely dissolve the cellulose sample. The intrinsic viscosity [η] of the dissolved cellulose solution was measured by a viscometer in a water bath at 25 ± 0.5 °C. The DP of the cellulose can be calculated based on formula (3):

$$\mathrm{DP}^{0.905} = 0.75[\eta] \quad (3)$$

where [η] is the measured intrinsic viscosity in mL/g.

Cellulose crystallinity was measured by X-ray diffraction (XRD). The fibers or fibril suspensions were evenly dispersed in water and then poured onto a filter to acquire sheets of fibers. The crystallinity index (CrI) of air-dried fiber or fibril sheets was measured by XRD analysis (D/max-IIIA, Japan) with Cu-Kα diffraction in the Bragg angle range, 2θ, of 5°-50°. CrI was determined based on Eq. (4) (Segal, Creely, Martin, & Conrad, 1959),

$$\mathrm{CrI} = (I_{200} - I_{am})/I_{200} \times 100\% \quad (4)$$

where I_{200} and I_{am} are the peak intensities at 2θ close to 22.6° and 18.6°, respectively.

2.7. CNF suspension rheology

Rheological properties of CNF suspensions were evaluated using a rotary rheometer (DHR-1, TA Instruments, New Castle, DE, USA) equipped with a parallel plate geometry with a diameter of 25 mm. The steady-state viscosity of CNF suspensions was measured in shear rates ranging from 0.01 to 1000 s^{-1}. Storage modulus (G′) and loss modulus

(G″) were measured over an angular frequency of 0.1–100 rad/s. All rheological measurements were performed at 25 °C.

The changes in the structure of CNF suspensions can be characterized by the oscillatory frequency dependent phase lag angle (δ) between the viscous and elastic components of the complex modulus, which can be expressed using Eq. (5) (Alves et al., 2020),

$$tan\ \delta = G''/G' \quad (5)$$

To better understand the rheological properties of CNF suspensions, Herschel-Bulkley model was used to depict the relationship between viscosity and shear rate as shown in Eq. (6) (Pakutsah & Aht-Ong, 2020),

$$\tau = \tau_0 + k\gamma^m \quad (6)$$

where, τ is shear stress in Pa; τ_0 represents shear yield stress in Pa, k is the viscosity coefficient in Pa•s^m, γ is shear rate in 1/s, and *m* is flow index.

2.8. Statistical analysis

One-way analysis of variance (ANOVA) using SPSS statistical software and Tamhane's test for unequal variances were conducted on measured fibril diameters. The reported data are averages ± standard deviation.

3. Results and discussion

3.1. Morphologies and properties of fibrils after SMC milling

The original unfibrillated BHKP fibers (Fig. 2A) have an average diameter of 16.9 μm. Fibers were subjected to compressive, shearing, and friction forces (Wang, Zhu, Gleisner, et al., 2012) during SMC milling, which resulted in external fibrillation as verified by the SEM images of coarsely fibrillated sample CsP1 (Fig. 2B-C). Hairs or fibrils were emanating from the fiber surface as a result of coarse fibrillation (Fig. 2B). However, the extent of fibrillation by coarse milling was low as indicated by the physical dimensions (comparing with the original BHKP fibers in Fig. 2A) and a small decrease in DP from 650 to 594 (Table 1), or by only 8.6 %. WRV values were increased from 79 % to 137 % (Table 1). The main purpose of milling using the coarse disks was to obtain uniform mixing of the BHKP suspension, to break up large fiber flocs and prevent clogging during milling using the pair of fine disks.

Internal fibrillation of fibers took place during milling using fine

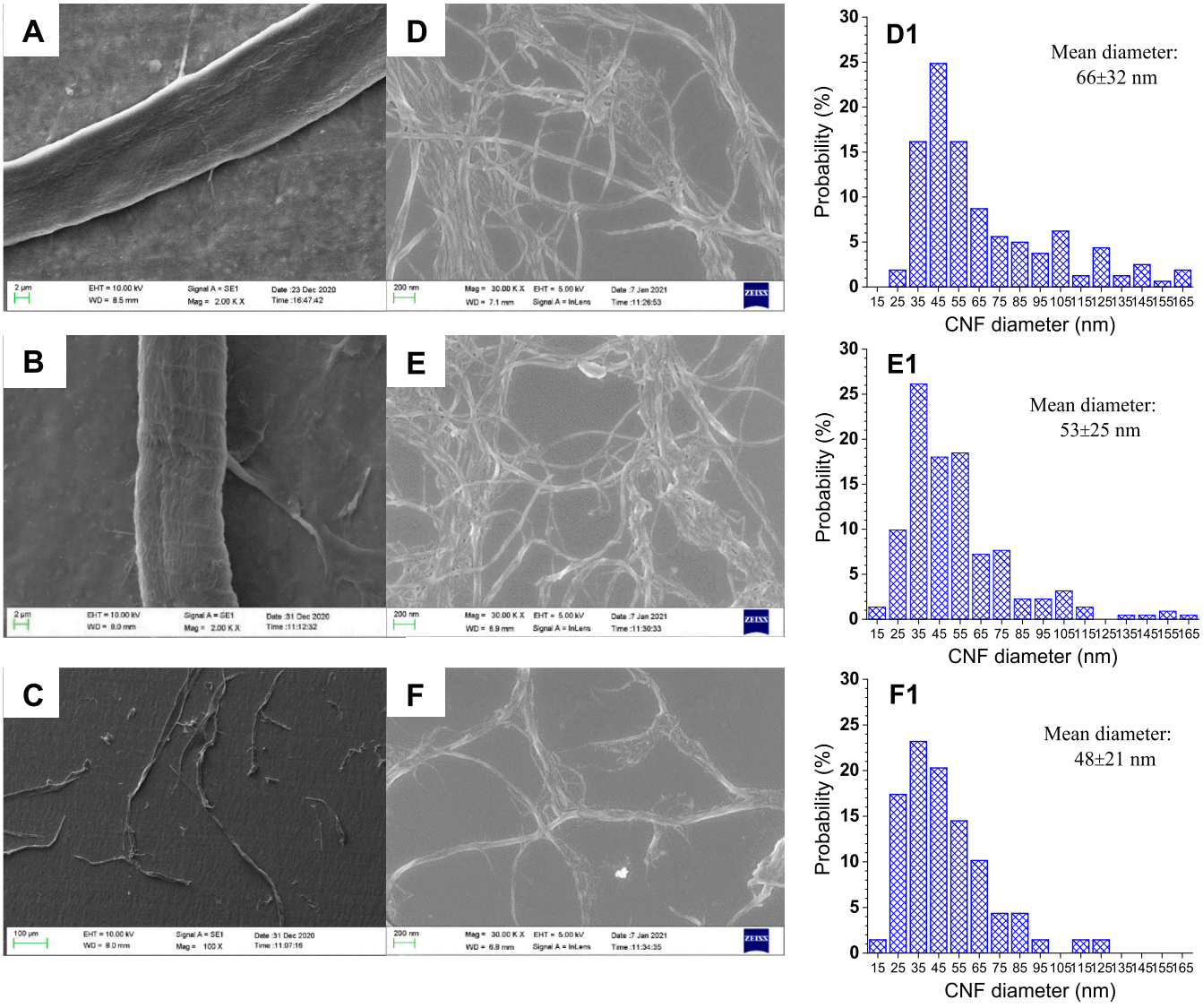

Fig. 2. SEM images of BHKP before and after SMC milling (A) Original BHKP, (B) and (C) CsP1 from coarse-disk milling, (D) FiP1, (E) FiP2, (F) FiP3 from fine-disk milling (scale bars = 200 nm), along with diameter distributions of FiP1 (D1), FiP2 (E1) and FiP3 (F1).

Table 1
EA, DP, and WRV of BHKP before and after SMC milling.

Samples	EA (mg/g)	DP	WRV (%)
Original BHKP	15.2 ± 2.6	650 ± 3	79 ± 2
CsP1	–	594 ± 3	137 ± 5
FiP1	30.4 ± 0.8	520 ± 5	317 ± 6
FiP2	33.6 ± 1.9	512 ± 8	334 ± 7
FiP3	38.6 ± 1.2	504 ± 4	381 ± 10

disks owing to the increase in compression force, which resulted in the break-up of the crosslinks between fibrils and delamination of S2 layer. The increase of abrasive shear and friction forces led to more significant external fibrillation and caused the split of the cell wall. Therefore, nanoscale fibrils were produced, (Fig. 2D-F; Fig. S1) (Wang, Zhu, Gleisner, et al., 2012) as directly observed from the SEM measured fibril diameter distributions (Fig. 2D1—F1). With increasing extent of milling, the diameter distribution shifted to the smaller diameters and the mean diameter was decreased from 66 nm (FiP1) after one pass through fine-disk-milling to 53 nm (FiP2), and 48 nm (FiP3), respectively, after two and three passes. The increase in the extent of fibrillation can be evaluated by EA (Gu et al., 2018). As listed in Table 1, EA of original BHKP was 15.2 mg/g, while EA of FiP1, FiP2 and FiP3 were 30.4 mg/g, 33.6 mg/g and 38.6 mg/g, respectively, indicating that SMC milling significantly increased the extent of fiber fibrillation with increasing extent of milling. In addition to EA, WRV can also reflect the extent of fibrillation (Gu et al., 2018; Wang & Cheng, 2009). As listed in Table 1, WRV of FiP1, FiP2 and FiP3 were 317 %, 330 % and 381 %, respectively, or 4.0, 4.2 and 4.8 times the WRV of the original fiber sample. Overall, the first pass fine milling resulted in the greatest increase in the extent of fibrillation based on EA and WRV data, i.e., the benefit of increasing milling, however, was diminished.

Shear force and friction force can cut fibers and shorten fibrils, though the shortening of fibril length and decreasing in fibril entanglement were not clearly reflected in the TEM images shown in Fig. 2D-F as the numbers of passes of milling was increased from one to three. However, they are reflected in the measured DP values of the fibrils shown. DP of fine-milled samples were 520 (FiP1), 512 (FiP2), and 504 (FiP3), decreased from 594 for the coarse-milled sample CsP1 (Table 1). It is worth noting that significant decrease in DP was not observed as the extent of fibrillation was increased, suggesting that the cutting effect of fine-disk SMC milling was minimal. Similar result was also observed by (Gu et al., 2018). Energy consumption, however, was increased from 5.5 to 10.5 kWh/kg (Fig. S2) with extended SMC milling from one to three passes. Therefore, FiP1 was selected as the starting material for post-fibrillation endoglucanase treatment in subsequent experiments.

3.2. *Effect of post-fibrillation endoglucanase treatment on CNF morphologies*

Endoglucanase can randomly cleave β-1,4 linkages in cellulose chains, thereby cutting the fibrils. DP of FiP1 and CsP1 decreased rapidly with increasing endoglucanase loading in the low dosage range, as shown in Fig. 3A. FiP1 with fine-disk milling had a steeper DP decrease with increasing endoglucanase dosage due to the increasing fibril surface area and cellulose accessibility to endoglucanase than CsP1 despite CsP1 having a longer treatment time of 24 h than 6 h for FiP1. DP of FiP1 and CsP1 decreased 63 % and 41 %, respectively, at the maximal endoglucanase dosage of 9 mg/g. However, DP for both samples reached an asymptotic value at endoglucanase loading of 3 mg/g, indicating that a low endoglucanase dosage was sufficient.

DP of FiP1 decreased from 520 to 299, or by 43 %, after endoglucanase treatment for 3 h at loading of 1 mg/g. Prolonged treatment time to 72 h further decreased DP to 202, or by 61 %, approaching the

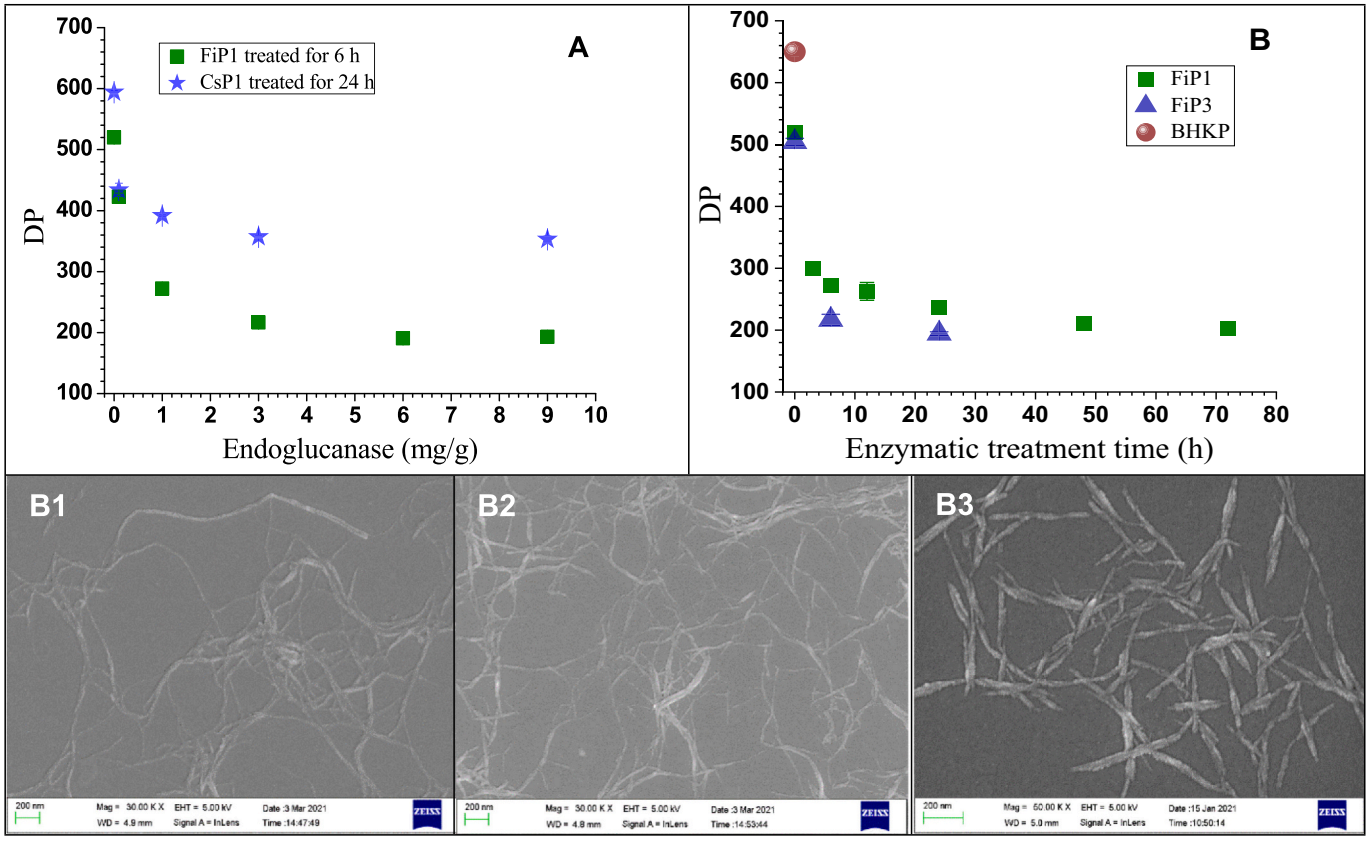

Fig. 3. The variation of cellulose DP with (A) endoglucanase dosage and (B) treatment time and fibrils morphologies at $t = 3$ h (B1), 12 h (B2), 72 h (B3) at cellulase endoglucanase loading of 1 mg/g.

asymptotic value, or level of degree of polymerization (LODP) (Battista, Coppick, Howsmon, Morehead, & Sisson, 1956) as shown in Fig. 3B. The decreases in fibril DP with enzymatic treatment time is clearly reflected in the fibril morphology shown by SEM images (Fig. 3B1-B3; Fig. S3). In addition, the percentage of total dissolved saccharides (monosaccharides and oligosaccharides) increased from 1.9 % (Po-P1E1t6) to 5.3 % (Po-P1E1t72) (Fig. S4), and solids yield was decreased from 99.0 % (Po-P1E1t6) to 94.8 % (Po- P1E1t72) (Table 2). The great CNF solids yield of approximately 95 % or higher indicate that fibers were simply shortened without significant hydrolysis to soluble sugars even with prolonged treatment time using post-fibrillation endoglucanase treatment. It appears that FiP3 from three passes of milling slightly reduced the endoglucanase treatment time to achieve the LODP of approximately 200. This is due to the slightly increased surface area resulting from additional passes of milling, which increased the amount of endoglucanase bound to cellulose fibrils (Table 1) and therefore accelerated the cleavage of β-1-4 glycosidic bonds.

Table 2
Yield, WRV and CrI of CNFs prepared by post-fibrillation and pre-fibrillation endoglucanase treatments.

Sample labels	Sample descriptions[a]	CNF yield (%)	WRV (%)	CrI (%)
BHKP	Bleached hardwood kraft pulp fibers	–	79 ± 2	54.8 ± 1.2
FiP1	BHKP after fine disk milled 1 pass	–	317 ± 6	51.4 ± 0.5
FiP2	BHKP after fine disk milled 2 passes			
FiP3	BHKP after fine disk milled 3 passes	–	381 ± 10	50.6 ± 0.4
Po-P1E1t3	FiP1 enzymatic treated for 3 h @E1	99.8 ± 0.6	282 ± 5	–
Po-P1E1t6	FiP1 enzymatic treated for 6 h @E1	99.0 ± 0.3	289 ± 9	–
Po-P1E1t12	FiP1 enzymatic treated for 12 h @E1	98.6 ± 0.2	281 ± 6	54.1 ± 1.4
Po-P1E1t24	FiP1 enzymatic treated for 24 h @E1	97.7 ± 0.9	278 ± 7	54.3 ± 0.9
Po-P1E1t48	FiP1 enzymatic treated for 48 h @E1	97.8 ± 0.8	292 ± 3	55.6 ± 0.8
Po-P1E1t72	FiP1 enzymatic treated for 72 h @E1	96.5 ± 0.4	290 ± 6	57.2 ± 1.2
Po-P1E01t6	FiP1 enzymatic treated for 6 h @E01	99.3 ± 0.3	–	–
Po-P1E3t6	FiP1 enzymatic treated for 6 h @E3	95.0 ± 0.4	–	–
Po-P1E6t6	FiP1 enzymatic treated for 6 h @E6	91.4 ± 0.6	–	–
Po-P1E9t6	FiP1 enzymatic treated for 6 h @E9	90.0 ± 0.5	–	–
Po-P2E1t6	FiP2 enzymatic treated for 6 h @E1	95.5 ± 0.6	–	–
Po-P2E1t12	FiP2 enzymatic treated for 12 h @E1	95.1 ± 0.5	–	–
Po-P2E1t24	FiP2 enzymatic treated for 24 h @E1	91.6 ± 0.4	–	–
Po-P3E1t6	FiP3 enzymatic treated for 6 h @E1	94.8 ± 0.8	–	–
Po-P3E1t12	FiP3 enzymatic treated for 12 h @E1	89.9 ± 0.4	–	–
Po-P3E1t24	FiP3 enzymatic treated for 24 h @E1	87.9 ± 0.9	345 ± 9	55.4 ± 0.8
Pre-E1t6	BHKP enzymatic pretreated for 6 h @E1	101.0 ± 0.5	–	–
Pre-E1t12	BHKP enzymatic pretreated for 12 h @E1	100.3 ± 0.2	–	–
Pre-E1t24	BHKP enzymatic pretreated for 24 h @E1	100.0 ± 0.1	99 ± 2	–
Pre-E1t24P1	Pre-E1t24 then fine disk milled 1 pass	–	338 ± 3	52.7 ± 0.7
Pre-E1t24P2	Pre-E1t24 then fine disk milled 2 passes	–	–	53.6 ± 0.4
Pre-E1t24P3	Pre-E1t24 then fine disk milled 3 passes	–	469 ± 8	49.8 ± 1.6

[a] Endoglucanase dosage: E01, E1, E3, E6, E9 = 0.1, 1, 3, 6, 9 mg protein/g fiber. Milled samples were subjected to course milling and fine milling with large gaps as described in Section 2.2 before fine milling with passes indicated at gap −100 μm.

SEM images and diameter distributions of CNFs prepared by post-fibrillation endoglucanase treatment for varied time are shown in Fig. 4 (also Fig. S5). By comparing with the sample before endoglucanase treatment (Fig. 2D and D1), it can be said that post-fibrillation endoglucanase treatment effectively reduced inter-fibril entanglement, fibril diameters, and the polydispersity of diameter distributions, in agreement with literature studies (Gourlay et al., 2018; Wang et al., 2016). The range of fibril diameter distribution was significantly decreased from approximately 165 nm for FiP1 (Fig. 2D1) to <100 nm after endoglucanase treatment (Fig. 4A1-C1), or the CNFs became more uniform in diameter with post-fibrillation endoglucanase treatment. Extending treatment time resulted in a smaller mean fibril diameter with a narrower distribution. Specifically, the mean diameter of FiP1 was 66 nm (Fig. 2D and D1) and reduced to 35 nm after endoglucanase treatment for just 3 h at loading of 1 mg/g (Fig. 4A and A1), and further decreased to 25 nm (Fig. 4C and C1) with 24 h treatment. Further extending enzymatic treatment time had negligible effect on fibril mean diameter (Fig. 4B and B1). Furthermore, increasing the extent of SMC milling prior to post-fibrillation enzymatic treatment did not affect the morphology of the enzymatically treated CNFs (comparing Fig. 4C and C1 (Po-P1E1t24) with Fig. 4D and D1 (Po-P3E1t24)).

Optical transmittance of a CNF suspension can provide qualitative information on the effect of post-fibrillation enzymatic treatment on the resultant CNF mean diameters (Nie et al., 2018; Wang & Zhu, 2015). The higher the transmittance, the smaller the representative mean fibril size is. The optical transmittances of the suspensions from endoglucanase pretreatment with subsequent milling, Pre-E1t24P1, Pre-E1t24P2 and Pre-E1t24P3, are all higher than that of FiP1, indicating that endoglucanase pretreatment did facilitate fibrillation to decrease CNF size (Fig. S6). However, the suspension of the CNFs from post-fibrillation endoglucanase treatment had a greater optical transmittance than the suspensions of the CNFs from endoglucanase pretreatment with the same extent of milling (Fig. S6). Increasing post-fibrillation enzymatic treatment time improved suspension transmittance or decreased representative mean fibril diameter, in agreement with SEM analysis shown in Fig. 4.

SEM images and diameter distributions of CNFs prepared by endoglucanase pretreatment with subsequent SMC milling were compared with those of CNFs from post-fibrillation endoglucanase treatment to verify the results from qualitative optical transmittance measurements discussed above. The comparisons, Fig. 4C and C1 with Fig. 4C' and C′1, and Fig. 4D and D1 with Fig. 4D' and D1, show that CNFs produced by endoglucanase pretreatment with subsequent SMC milling had a greater mean diameter and are more entangled than those of the CNFs from post-fibrillation endoglucanase treatment with the same extent of milling and enzyme treatment time at the same loading. It is noted that fibrillation energy consumption for producing Po-P1E1t24 (Fig. 4C and C1) through post-fibrillation enzymatic treatment was greater than that consumed to produce the corresponding CNF sample using enzymatic pretreatment Pre-E1t24P1 (Fig. 4C' and C′1) as illustrated in Fig. S2. However, even after three passes of fibrillation of the enzymatically pretreated sample in the SMC with more energy consumption than one pass without enzymatic pretreatment (Fig. S2), the resultant enzymatically pretreated CNF sample Pre-E1t24P3 (Fig. 4D' and D'1) remained coarser than Po-P1E1t24 (Fig. 4C and C'1) in terms of diameter distribution range and fibril entanglement. Therefore, post-fibrillation enzymatic treatment requires less energy input than enzymatic pretreatment to produce fibrils with equivalent morphology.

Our earlier study suggested that wood cell wall cellulose fibrils aggregate not only in the radial but also in the longitudinal direction to form coarse and long cellulosic fibers (Qin et al., 2016). Therefore,

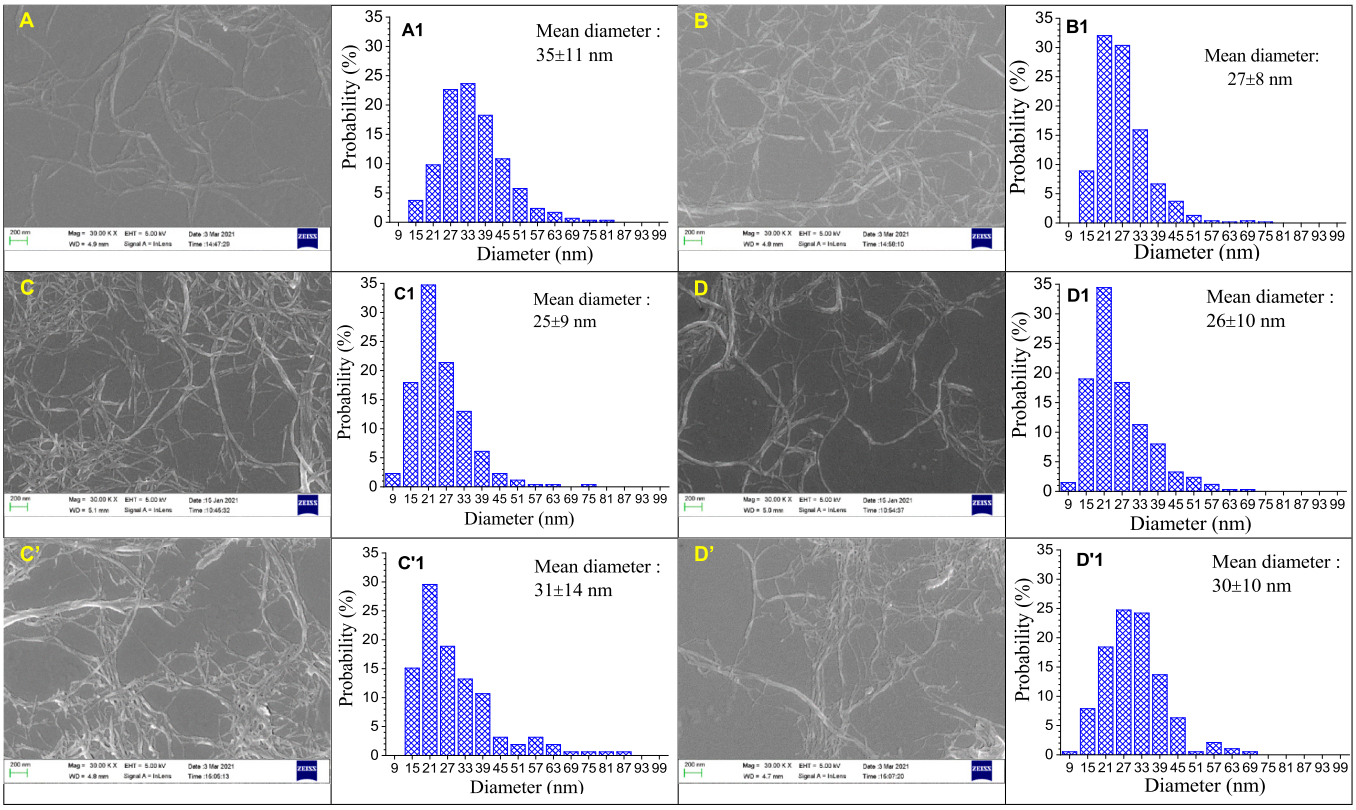

Fig. 4. SEM images and diameter distribution histograms of cellulose nanofibrils prepared by post-fibrillation endoglucanase treatment in comparison with those from endoglucanase pretreatment with equivalent subsequent fibrillation. (A, A1) Po-P1E1t3, (B, B1) Po-P1E1t48, (C, C1) Po-P1E1t24, (C′, C′1) Pre-E1t24P1, (D, D1) Po-P3E1t24, (D′, D′1) Pre-E1t24P3. All scale bars = 200 nm.

shortening fibril length is a necessary condition (Zhu & Agarwal, 2022) to produce thin fibrils as indirectly verified in literature using different chemical treatment methods on different wood fibers (Bian, Chen, Dai, & Zhu, 2017; Qin et al., 2016). Since cellulose DP can be a measure of CNF length, we plotted DP against SEM measured CNF diameters for the sample produced in this study. As shown clearly in Fig. 5, CNF mean diameters decreased with the decrease in cellulose DP for different CNF samples whether resulting from increasing the extent of fibrillation using more passes through the fine-milling disks in SMC, or from extending the duration of post-fibrillation endoglucanase treatment. In other words, cellulose depolymerization is necessary and can facilitate nanofibrillation for producing thin nanofibrils (Zhu & Agarwal, 2022). Post-fibrillation endoglucanase treatment can depolymerize cellulose through cleaving β-1,4 linkages, which releases thin constituent fibrils from fibril bundles or aggregates to result in a CNF sample with thinner mean diameter (Figs. 4 and 5). This mechanism illustrates the effectiveness of post-fibrillation enzymatic treatment for producing fine and uniform cellulose nanofibrils. The one-way ANOVA results confirmed that the differences in the average diameter among the six samples are significant, with $p = 0.000$ (<0.05), although the difference between FiP2 and FiP3 is not significant with $p = 0.923$ (>0.05).

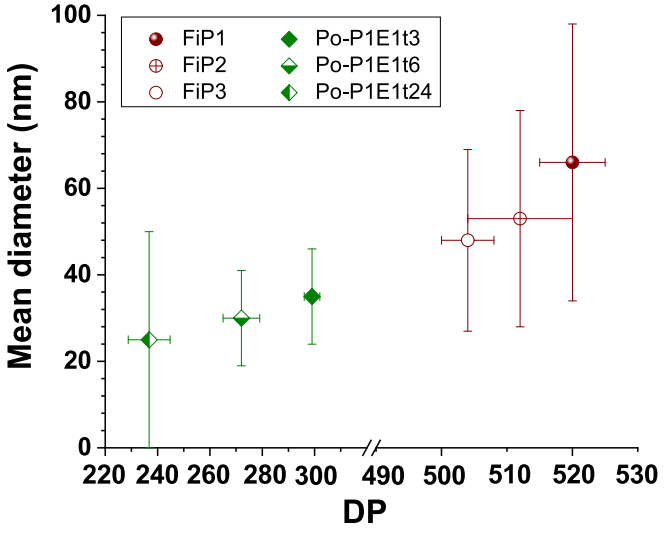

Fig. 5. Correlations between cellulose DP and CNF mean diameters from pure mechanical fibrillation and post-fibrillation endoglucanase treatment. Error bars were standard deviations.

3.3. *Effect of post-fibrillation endoglucanase treatment on WRV and CrI of CNFs*

WRV is a measure of the water-holding capacity of cellulose materials that includes the water in the pores and thin layer on outer surface of fibers or fibrils, particularly in the inter-fiber or inter-fibril meniscus (Gu et al., 2018; Luo, Zhu, Gleisner, & Zhan, 2011). It also can be a measure of the accessibility of cellulose materials to water or the total fibril surface area (Gu et al., 2018). As discussed earlier, WRV of BHKP was significantly increased from 79 % to 317 % (FiP1) and 381 % (FiP3) after SMC milling (Table 2). After post-fibrillation endoglucanase treatment of FiP1 for 3 to 72 h, WRV of the resultant samples Po-P1E1t3, Po-P1E1t6, Po-P1E1t12, Po-P1E1t24, Po-P1E1t48 and Po-P1E1t72 were decreased slightly to approximately 280 % with negligible difference (Table 2). This decrease is perhaps due to the cleavage of β-1,4 bonds by endoglucanase, which decreased fibril entanglement and therefore water-holding capacity in the inter-fibril meniscus. WRV of FiP3 was also slightly decreased to 345 % from 381 % after post-fibrillation

endoglucanase treatment for 24 h (Table 1).

X-ray diffractograms showed that all cellulosic samples exhibited the characteristic peaks of cellulose I at 2θ = 18 and 22.5° (Fig. S7). After post-fibrillation endoglucanase treatment, these characteristic peaks remained. As listed in Table 2, SMC milling reduced CrI from 54.8 % (original BHKP) to 51.4 % (FiP1) and 50.6 % (FiP3), respectively. Subsequent post-fibrillation endoglucanase treatment slightly increases CNF CrI due to the hydrolysis of paracrystalline cellulose. For example, CrI of Po-P1E1t12 was increased to 54.1 % with endoglucanase treatment at 1 mg/g for 12 h, slightly lower than that of original BHKP. With the increase in treatment time, the CNF CrI was increased. Similarly, CrI of Po-P3E1t24 was increased to 55.4 % after post-fibrillation endoglucanase treatment for 24 h. CrI of Pre-E1t24P1 and Pre-E1t24P3 were 52.7 % and 49.8 %, respectively, both lower than Po-P1E1t24 and Po-P3E1t24, both of which had the same endoglucanase loading of 1 mg/g and treated for 24 h. It was also lower than the CrI of untreated BHKP because the subsequent SMC grinding reduced CrI of fibers.

3.4. Rheological properties of post-fibrillation endoglucanase treated CNF suspensions

Rheological properties of CNF suspensions were characterized under steady and dynamic conditions to understand the viscoelastic properties of the suspensions. The suspension shear stress vs shear rate displayed a nonlinear relationship, especially at high CNF consistencies, and can be well fitted by the Herschel-Bulkley model ($\tau = \tau_0 + k\gamma^m$) as shown in Fig. S8. Flow indices (m) of all the CNF suspensions were <1 (Table S3), strongly supporting a shearing-thinning behavior. However, at CNF consistency of 0.5 wt%, the flow indices for suspensions FiP1, Po-P1E1t3, Po-P1E1t48 and Pre-E1t24P1 were all close to 1, i.e., a

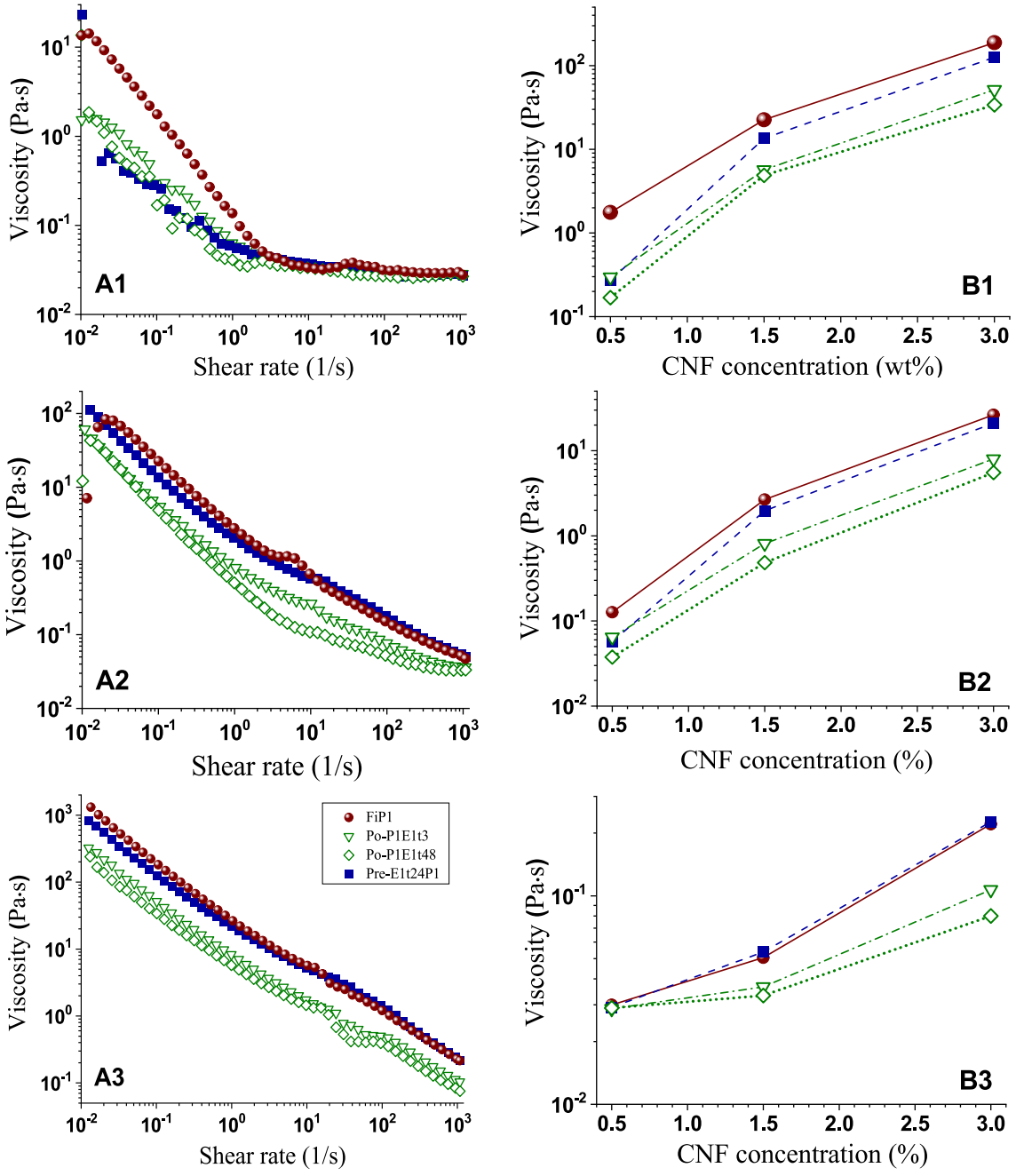

Fig. 6. Viscosity of CNF suspensions. Left column: Variation with shear rate at different CNF concentrations (A1) 0.5 wt%, (A2) 1.5 wt%, (A3) 3 wt%. Right column: Variation with CNF concentrations at different shear rates (B1) 0.1 1/s, (B2) 10 1/s and (B3) 1000 1/s.

Newtonian behavior. This is because the concentration of CNF suspensions was too low to result in observable deviations from water (a Newtonian fluid) in their rheological properties. At higher CNF consistencies of 1.5 wt% and 3.0 wt%, the shear stress of the suspension of Pre-E1t24P1 from enzymatic pretreatment were higher than the corresponding values of the suspensions of Po-P1E1t3 and Po-P1E1t48 (Fig. 6), both from post-fibrillation endoglucanase treatment at the same enzyme dosage. This is because the DP values (representative of fibril length) of Pre-E1t24P1 fibrils were greater than those of Po-P1E1t3 and Po-P1E1t48 due to lack of post-fibrillation endoglucanase cleavage (Table S3). The shear yield stress τ_0 is a typical rheological characteristic of CNF suspensions. Increasing the concentration of CNF (FiP1) suspension from 1.5 wt% to 3.0 wt%, τ_0 was increased from 2.38 Pa to 6.75 Pa (Table S3) due to the increasing fibril flocculation at a higher CNF consistency. Similar behavior was also observed from all CNF samples evaluated.

The rheological properties of CNF suspensions were closely related to the size of the fibrils and its dispersion microstructure (Li, Wu, et al., 2021). Increasing CNF concentration increased suspension viscosity, as shown in Fig. 6A1-A3, in agreement with literature (Li et al., 2015; Liao et al., 2021). Moreover, all CNF suspensions displayed typical shear-thinning behavior. The suspension showed high viscosity at very low shear rate because the entangled network of fibrils were resistant to flow. At higher shear rates, fibril structure was deformed and started to flow. Hence, the viscosity decreased (Gourlay et al., 2018). At a low shear rate of 0.1 1/s, the different CNFs FiP1, Po-P1E1t3, and Po-P1E1t48 showed different viscosities even at low concentrations of 0.5 % (Fig. 6A1). This difference disappeared with increasing shear rate. At shear rates >30 1/s, the viscosity of these three CNFs were essentially the same. Compared with Po-P1E1t3 (Fig. 4A) and Po-P1E1t48 (Fig. 4B), FiP1 (Fig. 2D) has the greatest DP values (Table 2), thus the fibrils were more likely to aggregate and intertwine with each other to form a more stable network structure (Liu et al., 2017; Qu, Wang, Li, & Wang, 2021; Wang et al., 2020). Increasing enzymatic treatment time resulted in short fibrils, which decreased viscosity; for example, the viscosity of Po-P1E1t48 was always lower than that of Po-P1E1t3 (Fig. 6A1-A3). Also note that the effect of enzymatic pretreatment on CNF suspension rheology was obvious only at low suspension consistency of 0.5 wt% (Fig. 6A1) and disappeared at high consistencies >1.5 wt% (Fig. 6A2-A3), while the effect of post-fibrillation enzymatic treatment remained at high suspension consistencies (Fig. 6B1—B3).

The storage modulus G′ describes the elastic behavior or gel-like characteristic of CNF suspensions, while the loss modulus G″ describes viscous behavior or liquid-like characteristics of CNF suspensions. In addition, G′ and G″ define the ability of a CNF suspension to reverse its deformation (Gaspard et al., 2021; Qu et al., 2021). As reported previously, CNFs are more likely to have gel-like behavior even at low concentrations (Li et al., 2015; Liao et al., 2021; Nechyporchuk et al., 2016). Transition from liquid-like to gel-like can occur at a low consistency of 0.5 wt% for TEMPO-oxidized CNF (Liao et al., 2021). This is observed in the present study. As shown in Fig. 7, CNF suspensions at 0.5 wt% under an oscillatory strain of 1.25 wt% were transitioned from liquid-like to gel-like, i.e., G′ greater than G″ ($\tan\delta > 1$), at a low angular frequency of below approximately 1.5 rad/s. This transition of suspension behavior from liquid-like to gel-like was thought to be due to extensive aggregation in the system, which results in the gelation (Shafiei-Sabet, Hamad, & Hatzikiriakos, 2014). The transition angular frequency had no visible variations among the four samples tested, indicating that the variations in the susceptivity of the CNF suspension to form gel was insignificant, perhaps due to the small variations in the morphology of these four samples, as shown in Fig. 2F and F1, Fig. 4A and A1, B and B1, and C' and C'1, respectively.

Although increasing suspension concentration can facilitate the formation of network and structure through non-covalent aggregations (Anvari & Joyner, 2017), other factors can affect the viscoelastic behavior of CNF suspensions as summarized in literature

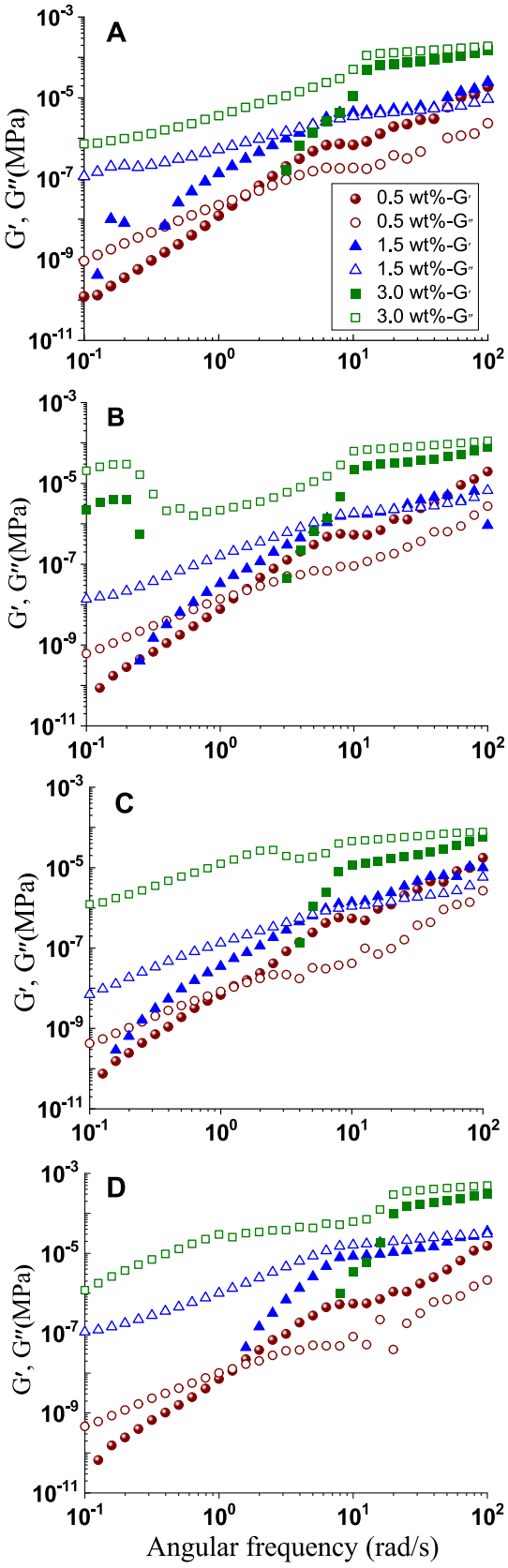

Fig. 7. Variation of storage modules (G', solid symbols) and loss module (G″, open symbols) of different CNF suspensions with respect to angular frequency. (A) FiP1, (B) Po-P1E1t3, (C) Po-P1E1t48 (D) Pre-E1t24P1.

(Nechyporchuk et al., 2016). Electrostatic repulsive interactions between fibrils induced by fibril surface charge can decrease the tendency of forming fibril networks. This repulsive force is enhanced by two factors: (1) the suspension concentration, because a higher suspension concentration results in a shorter mean distance between fibrils to increase fibril repulsion, and (2) the amount of fibril surface charge. Fibrils produced from chemically pretreated cellulose fibers, such as TEMPO-mediated oxidation (Isogai, Saito, & Fukuzumi, 2011), concentrated sulfuric acid (Wang, Zhu, Reiner, et al., 2012) and dicarboxylic acid (Chen, Zhu, Baez, Kitin, & Elder, 2016) hydrolysis tends to result in a more stable suspension due to increasing electrostatic repulsive interactions among fibrils as a result of surface carboxylation or sulfation. For the fibrils produced from enzymatic treatment without chemical modification in the present study, the fibril surface charge is native to wood cellulose fibers. The electrostatic repulsion can be enhanced at elevated fibril concentrations to result in a less gel-like suspension than that at low concentrations. This can be seen from the two sets of plots shown in Fig. 7, the suspension concentration of 3 wt% has the least gel-like behavior. It should be pointed out that fibril sedimentation, especially at high suspension concentrations, can decrease fibril concentration in the upper plate region of the parallel-plate rotary rheometer used in the present study (Nechyporchuk et al., 2016) to affect the measured viscoelastic behavior of CNF suspensions (Nechyporchuk et al., 2016).

4. Conclusions

This study investigated post-fibrillation endoglucanase treatment for preparation of CNFs. SEM imaging analysis revealed that post-fibrillation endoglucanase treatment can effectively reduce fibril network and entanglement by cutting fibrils through depolymerizing cellulose, as validated by the measured DP values. Post-fibrilltion endoglucanase treatment also reduced fibril mean diameter even at a low dosage of 1 mg/g. As a result, post-fibrillation endoglucanase treatment can produce uniform CNFs. Furthermore, post-fibrillation enzymatic treatment uses less energy for mechanical fibrillation than enzymatic pretreatment with subsequent mechanical fibrillation for producing CNFs with equivalent morphologies. A typical enzymatic treatment time is approximately 12–24 h. Post-fibrillation endoglucanase treatment modifies the rheology of the resultant CNF suspension by reducing the viscosity of the suspension at a wide range of shear rate from 0.001 to 1000 1/s. The flow indices of all CNFs suspensions were <1, indicating a pseudoplastic fluid behavior.

CRediT authorship contribution statement

Wang conducted the experiments and drafted the paper. Zeng advised Wang in experiments and manuscript writing. Zhu initiated the research project and advised the experiments as well as conducted detailed revision of the manuscript.

Declaration of competing interest

The authors declare that they do not have competing interests for the work reported here.

Data availability

Data will be made available on request.

Acknowledgments

The authors would like to acknowledge financial support from USDA Forest Products Laboratory and Chinese Scholarship Council (CSC), Characterization and Instrument Development of Cross-Scale Nanofiber Based on Microfluidic Technology (2020ZD01), National Key Research and Development Program of China (Number: 2017YFB0307902), the Fundamental Research Funds for the Central Universities (2019MS085) and Guangdong Provincial Key Laboratory of Plant Resources Biorefinery (2021B1212040011).

Appendix A. Supplementary data

Supplementary data to this article can be found online at https://doi.org/10.1016/j.carbpol.2022.119885.

References

Aarstad, O., Heggset, E. B., Pedersen, I. S., Bjørnøy, S. H., Syverud, K., & Strand, B. L. (2017). Mechanical properties of composite hydrogels of alginate and cellulose nanofibrils. *Polymers, 9*(8), 378.

Alves, L., Ferraz, E., Lourenco, A. F., Ferreira, P. J., Rasteiro, M. G., & Gamelas, J. A. F. (2020). Tuning rheology and aggregation behaviour of TEMPO-oxidised cellulose nanofibrils aqueous suspensions by addition of different acids. *Carbohydrate Polymers, 237*, Article 116109.

Anderson, S. R., Esposito, D., Gillette, W., Zhu, J. Y., Baxa, U., & McNeil, S. E. (2014). Enzymatic preparation of nanocrystalline and microcrystalline cellulose. *Tappi Journal, 13*(5), 35–42.

Anvari, M., & Joyner, H. S. (2017). Effect of formulation on structure-function relationships of concentrated emulsions: Rheological, tribological, and microstructural characterization. *Food Hydrocolloids, 72*, 11–26.

Arantes, V., Dias, I. K. R., Berto, G. L., Pereira, B., Marotti, B. S., & Nogueira, C. F. O. (2020). The current status of the enzyme-mediated isolation and functionalization of nanocelluloses: Production, properties, techno-economics, and opportunities. *Cellulose, 27*(18), 10571–10630.

Battista, O. A., Coppick, S., Howsmon, J. A., Morehead, F. F., & Sisson, W. A. (1956). Level-off degree of polymerization: Relation to polyphase structure of cellulose fibers. *Industrial and Engineering Chemistry, 48*(2), 333–335.

Bian, H., Chen, L., Dai, H., & Zhu, J. Y. (2017a). Effect of fiber drying on properties of lignin containing cellulose nanocrystals and nanofibrils produced through maleic acid hydrolysis. *Cellulose, 24*(10), 4205–4216.

Bian, H., Chen, L., Gleisner, R., Dai, H., & Zhu, J. Y. (2017b). Producing wood-based nanomaterials by rapid fractionation of wood at 80 °C using a recyclable acid hydrotrope. *Green Chemistry, 19*(14), 3370–3379.

Bian, H., Dong, M., Chen, L., Zhou, X., Ni, S., Fang, G., & Dai, H. (2019). Comparison of mixed enzymatic pretreatment and post-treatment for enhancing the cellulose nanofibrillation efficiency. *Bioresource Technology, 293*, Article 122171.

Bradford, M. M. (1976). A rapid and sensitive method for the quantitation of microgram quantities of proteins utilizing the principle of protein dye binding. *Nature, 227*(1–2), 248–254.

Cai, C., Hirth, K., Gleisner, R., Lou, H., Qiu, X., & Zhu, J. Y. (2020). Maleic acid as a dicarboxylic acid hydrotrope for sustainable fractionation of wood at atmospheric pressure and $\leq$ 100 °C: Mode and utility of lignin esterification. *Green Chemistry, 22*(5), 1605–1617. https://doi.org/10.1039/C9GC04267A

Chen, L., Zhu, J. Y., Baez, C., Kitin, P., & Elder, T. (2016). Highly thermal-stable and functional cellulose nanocrystals and nanofibrils produced using fully recyclable organic acids. *Green Chemistry, 18*, 3835–3843.

Filson, P. B., Dawson-Andoh, B. E., & Schwegler-Berry, D. (2009). Enzymatic-mediated production of cellulose nanocrystals from recycled pulp. *Green Chemistry, 11*(11), 1808–1814.

Gaspard, S. J., Sharma, P., Fitzgerald, C., Tobin, J. T., O'Mahony, J. A., Kelly, A. L., & Brodkorb, A. (2021). Influence of chaperone-like activity of caseinomacropeptide on the gelation behaviour of whey proteins at pH 6.4 and 7.2. *Food Hydrocolloids, 112*, Article 106249.

Gourlay, K., Van Der Zwan, T., Shourav, M., & Saddler, J. (2018). The potential of endoglucanases to rapidly and specifically enhance the rheological properties of micro/nanofibrillated cellulose. *Cellulose, 25*(2), 977–986.

Gu, F., Wang, W., Cai, Z., Xue, F., Jin, Y., & Zhu, J. Y. (2018). Water retention value for characterizing fibrillation degree of cellulosic fibers at micro and nanometer scales. *Cellulose, 25*, 2861–2871.

Heggset, E. B., Aaen, R., Veslum, T., Henriksson, M., Simon, S., & Syverud, K. (2020). Cellulose nanofibrils as rheology modifier in mayonnaise - a pilot scale demonstration. *Food Hydrocolloids, 108*.

Henriksson, M., Henriksson, G., Berglund, L. A., & Lindstrom, T. (2007). An environmentally friendly method for enzyme-assisted preparation of microfibrillated cellulose (MFC) nanofibers. *European Polymer Journal, 43*(8), 3434–3441.

Henrique, M. A., Neto, W. P. F., Silvério, H. A., Martins, D. F., Gurgel, L. V. A., da Silva Barud, H., de Morais, L. C., & Pasquini, D. (2015). Kinetic study of the thermal decomposition of cellulose nanocrystals with different polymorphs, cellulose I and II, extracted from different sources and using different types of acids. *Industrial Crops Products, 76*, 128–140.

Hoeger, I. C., Nair, S. S., Ragauskas, A. J., Deng, Y., Rojas, O. J., & Zhu, J. Y. (2013). Mechanical deconstruction of lignocellulose cell walls and their enzymatic saccharification. *Cellulose, 20*(2), 807–818.

Hu, C., Zhao, Y., Li, K., Zhu, J. Y., & Gleisner, R. (2015). Optimizing cellulose fibrillation for the production of cellulose nanofibrils by a disk grinder. *Holzforschung, 69*(8), 993–1000.

Hu, J., Tian, D., Renneckar, S., & Saddler, J. N. (2018). Enzyme mediated nanofibrillation of cellulose by the synergistic actions of an endoglucanase, lytic polysaccharide monooxygenase (LPMO) and xylanase. *Scientific Reports, 8*(1), 3195.

Isogai, A., Saito, T., & Fukuzumi, H. (2011). TEMPO-oxidized cellulose nanofibers. *Nanoscale, 3*(1), 71–85.
Iwamoto, S., Nakagaito, A. N., & Yano, H. (2007). Nano-fibrillation of pulp fibers for the processing of transparent nanocomposites. *Applied Physics A: Materials Science & Processing, 89*(2), 461–466.
Khan, A., Wang, B., & Ni, Y. (2020). Chitosan-nanocellulose composites for regenerative medicine applications. *Current Medicinal Chemistry, 27*(28), 4584–4592.
Koskela, S., Wang, S., Xu, D., Yang, X., Li, K., Berglund, L. A., McKee, L. S., Bulone, V., & Zhou, Q. (2019). Lytic polysaccharide monooxygenase (LPMO) mediated production of ultra-fine cellulose nanofibres from delignified softwood fibres. *Green Chemistry, 21*(21), 5924–5933.
Li, M. C., Wu, Q., Moon, R. J., Hubbe, M. A., & Bortner, M. J. (2021a). Rheological aspects of cellulose nanomaterials: Governing factors and emerging applications. *Advanced Materials, 33*(21), Article 2006052.
Li, M.-C., Wu, Q., Song, K., Lee, S., Qing, Y., & Wu, Y. (2015). Cellulose nanoparticles: Structure-morphology-rheology relationships. *ACS Sustainable Chemistry and Engineering, 3*(5), 821–832.
Li, T., Chen, C., Brozena, A. H., Zhu, J. Y., Xu, L., Driemeier, C., Dai, J., Rojas, O. J., Isogai, A., Wagberg, L., & Hu, L. (2021b). Developing fibrillated cellulose as a sustainable technological material. *Nature, 590*(7844), 47–56.
Liao, J., Pham, K. A., & Breedveld, V. (2021). TEMPO-CNF suspensions in the viscoelastic regime: Capturing the effect of morphology and surface charge with a rheological parameter. *Cellulose, 28*(2), 813–827.
Liu, C., Du, H., Dong, L., Wang, X., Zhang, Y., Yu, G., Li, B., Mu, X., Peng, H., & Liu, H. (2017). Properties of nanocelluloses and their application as rheology modifier in paper coating. *Industrial Engineering Chemistry Research, 56*(29), 8264–8273.
Luo, X., Zhu, J., Gleisner, R., & Zhan, H. (2011). Effects of wet-pressing-induced fiber hornification on enzymatic saccharification of lignocelluloses. *Cellulose, 18*(4), 1055–1062.
Mandal, A., & Chakrabarty, D. (2011). Isolation of nanocellulose from waste sugarcane bagasse (SCB) and its characterization. *Carbohydrate Polymers, 86*(3), 1291–1299.
Nechyporchuk, O., Belgacem, M. N., & Pignon, F. (2016). Current progress in rheology of cellulose nanofibril suspensions. *Biomacromolecules, 17*(7), 2311–2320.
Nie, S., Zhang, K., Lin, X., Zhang, C., Yan, D., Liang, H., & Wang, S. (2018). Enzymatic pretreatment for the improvement of dispersion and film properties of cellulose nanofibrils. *Carbohydrate Polymers, 181*, 1136–1142.
Paakko, M., Ankerfors, M., Kosonen, H., Nykanen, A., Ahola, S., Osterberg, M., Ruokolainen, J., Laine, J., Larsson, P. T., Ikkala, O., & Lindstrom, T. (2007). Enzymatic hydrolysis combined with mechanical shearing and high-pressure homogenization for nanoscale cellulose fibrils and strong gels. *Biomacromolecules, 8*(6), 1934–1941.
Pakutsah, K., & Aht-Ong, D. (2020). Facile isolation of cellulose nanofibers from water hyacinth using water-based mechanical defibrillation: Insights into morphological, physical, and rheological properties. *International Journal of Biological Macromolecules, 145*, 64–76.
Qin, Y., Qiu, X., & Zhu, J. Y. (2016). Understanding longitudinal wood fiber ultra-structure for producing cellulose nanofibrils using disk milling with diluted acid prehydrolysis. *Scientific Reports, 6*(35602).
Qu, R., Wang, Y., Li, D., & Wang, L. (2021). The study of rheological properties and microstructure of carboxylated nanocellulose as influenced by level of carboxylation. *Food Hydrocolloids, 121*, Article 106985.
Questell-Santiago, Y. M., Zambrano-Varela, R., Amiri, M. T., & Luterbacher, J. S. (2018). Carbohydrate stabilization extends the kinetic limits of chemical polysaccharide depolymerization. *Nature Chemistry, 10*(12), 1222–1228.
Sacui, I. A., Nieuwendaal, R. C., Burnett, D. J., Stranick, S. J., Jorfi, M., Weder, C., Foster, E. J., Olsson, R. T., & Gilman, J. W. (2014). Comparison of the properties of cellulose nanocrystals and cellulose nanofibrils isolated from bacteria, tunicate, and wood processed using acid, enzymatic, mechanical, and oxidative methods. *ACS Applied Materials and Interfaces, 6*(9), 6127–6138.
Saito, T., Hirota, M., Tamura, N., Kimura, S., Fukuzumi, H., Heux, L., & Isogai, A. (2009). Individualization of nano-sized plant cellulose fibrils by direct surface carboxylation using TEMPO catalyst under neutral conditions. *Biomacromolecules, 10*(7), 1992–1996.
Segal, L., Creely, J. J., Martin, A., Jr., & Conrad, C. (1959). An empirical method for estimating the degree of crystallinity of native cellulose using the X-ray diffractometer. *Textile Research Journal, 29*(10), 786–794.
Sehaqui, H., Kulasinski, K., Pfenninger, N., Zimmermann, T., & Tingaut, P. (2017). Highly carboxylated cellulose nanofibers via succinic anhydride esterification of wheat fibers and facile mechanical disintegration. *Biomacromolecules, 18*(1), 242–248.
Shafiei-Sabet, S., Hamad, W., & Hatzikiriakos, S. (2014). Ionic strength effects on the microstructure and shear rheology of cellulose nanocrystal suspensions. *Cellulose, 21*(5), 3347–3359.
Sluiter, A., Hames, B., Ruiz, R., Scarlata, C., Sluiter, J., Templeton, D., Sluiter, A., Hames, B., Ruiz, R., & Scarlata, C. (2006). *Determination of sugars, byproducts, and degradation products in liquid fraction process samples*. <sb:contribution><sb:title>National Renewable Energy</sb:title></sb:contribution><sb:host><sb:issue><sb:series><sb:title> Laboratory</sb:title></sb:series></sb:issue></sb:host>.
Spence, K. L., Venditti, R. A., Rojas, O. J., Habibi, Y., & Pawlak, J. J. (2011). A comparative study of energy consumption and physical properties of microfibrillated cellulose produced by different processing methods. *Cellulose, 18*(4), 1097–1111.
Squinca, P., Bilatto, S., Badino, A. C., & Farinas, C. S. (2020). Nanocellulose production in future biorefineries: An integrated approach using tailor-made enzymes. *ACS Sustainable Chemistry & Engineering, 8*(5), 2277–2286.
Tenhunen, T.-M., Peresin, M. S., Penttila, P. A., Pere, J., Serimaa, R., & Tammelin, T. (2014). Significance of xylan on the stability and water interactions of cellulosic nanofibrils. *Reactive & Functional Polymers, 85*, 157–166.
Villada, Y., Iglesias, M. C., Olivares, M. L., Casis, N., Zhu, J., Peresin, M. S., & Estenoz, D. (2021). Di-carboxylic acid cellulose nanofibril (DCA-CNF) as an additive in water-based drilling fluids (WBMs) applied to shale formations. *Cellulose, 28*(1), 417–436.
Wan, J., Lian, J., Wang, Y., & Ma, Y. (2015). Investigation of cellulose supramolecular structure changes during conversion of waste paper in near-critical water on producing 5-hydroxymethyl furfural. *Renewable Energy, 80*, 132–139.
Wang, H., Zhu, J. J., Ma, Q., Agarwal, U. P., Gleisner, R., Reiner, R., Baez, C., & Zhu, J. Y. (2020). Pilot-scale production of cellulosic nanowhiskers with similar morphology to cellulose nanocrystals. *Frontiers in Bioengineering and Biotechnology, 8*, Article 565084.
Wang, Q., Zhu, J., Gleisner, R., Kuster, T., Baxa, U., & McNeil, S. (2012a). Morphological development of cellulose fibrils of a bleached eucalyptus pulp by mechanical fibrillation. *Cellulose, 19*(5), 1631–1643.
Wang, Q., & Zhu, J. Y. (2015). Facile preparation of nanofiller-paper using mixed office paper without deinking. *Tappi Journal, 14*(3), 167–174.
Wang, Q. Q., Zhu, J. Y., Reiner, R. S., Verrill, S. P., Baxa, U., & McNeil, S. E. (2012b). Approaching zero cellulose loss in cellulose nanocrystal (CNC) production: Recovery and characterization of cellulosic solid residues (CSR) and CNC. *Cellulose, 19*(6), 2033–2047.
Wang, R., Chen, L., Zhu, J. Y., & Yang, R. (2017). Tailored and integrated production of carboxylated cellulose nanocrystals (CNC) with nanofibrils (CNF) through maleic acid hydrolysis. *ChemNanoMat, 3*(5), 328–335.
Wang, S., & Cheng, Q. (2009). A novel process to isolate fibrils from cellulose fibers by high-intensity ultrasonication, part 1: Process optimization. *Journal of Applied Polymer Science, 113*(2), 1270–1275.
Wang, W., Mozuch, M. D., Sabo, R. C., Kersten, P., Zhu, J. Y., & Jin, Y. (2016). Endoglucanase post-milling treatment for producing cellulose nanofibers from bleached eucalyptus fibers by a supermasscolloider. *Cellulose, 23*(3), 1859–1870.
Williams, N. X., Bullard, G., Brooke, N., Therien, M. J., & Franklin, A. D. (2021). Printable and recyclable carbon electronics using crystalline nanocellulose dielectrics. *Nature Electronics, 4*(4), 261–268.
Xu, Y., Yang, S., Zhao, P., Wu, M., Song, X., & Ragauskas, A. J. (2021). Effect of endoglucanase and high-pressure homogenization post-treatments on mechanically grinded cellulose nanofibrils and their film performance. *Carbohydrate Polymers, 253*, Article 117253.
Yarbrough, J. M., Zhang, R., Mittal, A., Wall, T. V., Bomble, Y. J., Decker, S. R., Himmel, M. E., & Ciesielski, P. N. (2017). Multifunctional cellulolytic enzymes outperform processive fungal cellulases for coproduction of nanocellulose and biofuels. *ACS Nano, 11*(3), 3101–3109.
Yousefi, H., Azad, S., Mashkour, M., & Khazaeian, A. (2018). Cellulose nanofiber board. *Carbohydrate Polymers, 187*, 133–139.
Zhou, H., St John, F., & Zhu, J. Y. (2019). Xylanase pretreatment of wood fibers for producing cellulose nanofibrils: A comparison of different enzyme preparations. *Cellulose, 26*(1), 543–555.
Zhu, J. Y., & Agarwal, U. P. (2022). Nanocellulose: Native state, production, and characterization. In F. Jiang, & L. Hu (Eds.), *Emerging nanotechnologies in nanocellulose*. New York: Springer Nature.
Zhu, J. Y., Agarwal, U. P., Ciesielski, P. N., Himmel, M. E., Gao, R., Deng, Y., Morits, M., & Osterberg, M. (2021). Towards sustainable production and utilization of plant-biomass-based nanomaterials: A review and analysis of recent developments. *Biotechnology for Biofuels, 14*(1), 114.
Zhu, J. Y., Sabo, R., & Luo, X. (2011). Integrated production of nano-fibrillated cellulose and cellulosic biofuel (ethanol) by enzymatic fractionation of wood fibers. *Green Chemistry, 13*(5), 1339–1344.